GEOPHYSICAL RESEARCH LETTERS, VOL. 27, NO. 17, PAGES 2645-2648, SEPTEMBER 1, 2000

Upper Tropospheric Humidity and Thin Cirrus

Brad J. Sandor[1,2], Eric J. Jensen[3], Elizabeth M. Stone[3], William G. Read[4], Joe W. Waters[4], John L. Mergenthaler[5]

Abstract. Upper tropospheric water vapor data from the UARS Microwave Limb Sounder (MLS) are compared with coincident optically thin (often subvisible) cirrus cloud measurements from the UARS Cryogenic Limb Array Etalon Spectrometer (CLAES) at 147 hPa in the tropics. A strong correlation is found between mean relative humidity with respect to ice (RHI) and percent occurrence of cirrus clouds. The cloudiness - RHI relationship is established from the coincident CLAES and MLS observations (Oct. 1991-May 1993), and used with 1991-97 MLS data to find by proxy the percent occurrence of cirrus for 1993-97. Interannual variability of cloudiness is investigated with the extended (1991-97) cirrus data, and a clear El Nino signature is seen. The observed relationship of RHI and optically thin cirrus provides a potential diagnostic of climatological behavior of atmospheric models, in which cirrus is important for radiative balance, heterogeneous chemistry, and the near-tropopause water budget.

1. Introduction

Water vapor is the most important greenhouse gas [*Jones and Mitchell*, 1991], and it influences surface radiative forcing most strongly from the upper troposphere [*Udelhofen and Hartmann*, 1995]. Global data from the Upper Atmospheric Research Satellite (UARS) MLS [*Barath et al.*, 1993] instrument indicate very high relative humidities in the tropical upper troposphere (147±30 hPa, 14.5±1.7 km). MLS-observed zonal-mean values of relative humidity with respect to ice at 147 hPa are 85% for latitudes 10°S-10°N [*Jensen et al.*, 1999], and 50% for 30°S-30°N [*Sandor et al.*, 1998]. MLS observation methods are discussed in section 2.

Wang et al. [1996] describe SAGE II observations of upper tropospheric clouds. They group these clouds into two categories: SAGE II measurable and SAGE II opaque, according to whether the observed clouds have 1 μm extinctions within the measurement range of SAGE II (extinction 0.0002-0.02 km^{-1}) or beyond that limit (>0.02 km^{-1}), respectively. SAGE II measurable clouds [*Wang et al.*, 1996] closely correspond to the *Sassen and Cho* [1992] category "subvisual clouds", which have optical depths $0.0002 < \tau < 0.03$. These subvisual clouds are so named because they are not visually observed from the ground. For example, *Wang et al.* [1996] find their SAGE II opaque cloud climatology is similar in distribution to, and has greater occurrence frequency than, the *Warren et al.* [1986; 1988] cirrus climatology determined from ground-based observations. From this, they argue the SAGE II measurable clouds are generally not seen by ground based observers - they are subvisible. This is consistent with the correspondence between *Sassen and Cho*'s [1992] subvisual clouds and *Wang et al.*'s [1996] SAGE II measurable clouds. *Wang et al.*'s [1996] "SAGE II opaque clouds" include both the *Sassen and Cho* [1992] categories "thin cirrus" and "opaque cirrostratus".

Mergenthaler et al. [1999] find good agreement between the SAGE II measurable (subvisible) climatology and the CLAES cloud data, and conclude that CLAES detects both subvisible and visible cirrus. The higher frequency of subvisible than visible cirrus implies the CLAES cloud detections are dominated by subvisible clouds. Near the equator at 15 km (the region addressed in this paper), *Wang et al.* [1996] find subvisible clouds in 45%, but SAGE II opaque (visible from the ground) clouds in <10%, of SAGE II measurements.

Optically thin cirrus are themselves radiatively important. *Jensen et al.* [1999] show the decrease in outgoing longwave radiation due to thin cirrus cloud is comparable to or greater than the decrease in outgoing longwave radiation due to the large water vapor abundances observed with MLS. Because optically thin cirrus are often not observable from the ground, understanding their global radiative effects requires use of satellite measures of cloud occurrence frequency, distribution, and variability.

For its 19 months of operation, CLAES upper tropospheric aerosol extinction data provide a measure of thin cirrus [*Mergenthaler et al.*, 1999], made in near spatial coincidence with MLS RHI observations. In section 3, we present an empirical functional dependence of the CLAES-measured frequency of cirrus cloud occurrence on the MLS-measured RHI mean values. From this functional dependence, we argue that MLS measurements can be used as a proxy for occurrence frequency of cirrus clouds. This is important because it extends the 19 months of CLAES measurements to over 5 years of direct and inferred cirrus data. Further, it establishes a diagnostic for model validation, in that means of the model cirrus, and cirrus vs RHI, behavior must be consistent with observations. As an example of the extended cirrus data set's utility, we analyze tropical 147 hPa cirrus interannual variation for 1991-97, with emphasis on the difference in cirrus distribution between the 1992-93 El Nino warm phase and 1995-96 neutral phase. *Massie et al.* [2000] use HALOE observations in a similar study of El Nino and tropical cirrus. CLAES/MLS data are complementary to HALOE and SAGE II: CLAES/MLS has coarser altitude resolution (3 km vs 1 km), but greater measurement frequency (1300 vs 30 altitude profiles/day) and thus better horizontal resolution than HALOE and SAGE II.

[1]National Center for Atmospheric Research, Boulder, CO
[2]Now at Space Science Institute, Boulder, CO
[3]NASA Ames Research Center, Moffett Field, CA
[4]Jet Propulsion Laboratory, California Institute of Technology, Pasadena
[5]Lockheed Palo Alto Research Laboratory, Palo Alto, CA

Paper number 1999GL011194.
0094-8276/00/1999GL011194$05.00

2. Observations

CLAES and MLS look generally in the same direction from UARS, with measurement tracks separated by <30 seconds and <200 km along-track at all times [*W.G. Read et al., manuscript in preparation,* 2000]. Both limb-scanning instruments measure atmospheric emission (CLAES in the infrared [*Roche et al.*, 1993] and MLS at mm wavelengths [*Barath et al.*, 1993, *Waters et al.,* 1999]). Measurements are retrieved on a subset of the standard UARS "level 3" profile surfaces, defined as pressure surfaces where $P = 10^{3-N/6}$ hPa and integer values of N. Measurements discussed in the present work are all from the 147 hPa surface (N=5). The CLAES instrument operated from Sept. 1991 until May 1993, when its cryogenic coolant was depleted. MLS data discussed in this paper were collected from Sept. 1991 until June 1997, when UARS battery failure led to degradation of the instrument pointing information. Beginning in 1995, MLS observation frequency decreased due to UARS power and MLS scan problems.

Read et al. [1995] present a preliminary retrieval of the MLS upper tropospheric humidity (UTH) measurements. The improved (and most recent) MLS retrieval version, V490, is described fully by *W.G. Read et al., manuscript in preparation,* [2000], and more briefly by *Stone et al.* [2000]. MLS measures radiances from Earth's limb as a function of tangent altitude of the observation line of sight. A nonlinear inversion algorithm is used to retrieve altitude profiles of water vapor from the measurements of radiance vs tangent altitude. The retrieval includes effects of dry and wet atmospheric absorption continua, refraction, and field of view. Estimated uncertainty and vertical resolution depend on the water vapor profile. Typical single profile uncertainty at 147 hPa is 20% relative humidity with respect to ice (RHI), or 8 ppmv mixing ratio. Uncertainties in averages over many profiles are much smaller [e.g. *Sandor et al.,* 1998]. *W.G. Read et al.* [*manuscript in preparation,* [2000] find a 0.91 correlation coefficient between coincident MLS and frost point hygrometer (balloon) measurements at 147 hPa, with MLS biased 12% drier than balloon values. Single profile precision is better than 5% RHI. Vertical resolution is typically 2.7 km (set by the number of retrieval points) but degrades to 4 km (the correlation length of the a priori profile) for RHI>90%. Horizontal resolution is 100 km along the line of sight, set by limb viewing geometry. While MLS spatial resolution is coarser than small-scale variations in water vapor, it is finer in the vertical than nadir-sounding instruments, and its high measurement frequency (1300 profiles per day) leads to better horizontal resolution than solar occultation instruments.

MLS water vapor data are retrieved and reported in units of relative humidity with respect to ice (RHI). A strength of MLS is that its insensitivity to ice aerosol allows measurements even in the presence of cirrus clouds. However, cirrus ice does contribute to MLS's signal, with about half the strength of water vapor per unit mass. For example, a measured RHI value of 200% indicates both saturated conditions and cirrus ice are present, and does not indicate 100% supersaturation. The MLS alone can not be used to infer supersaturation values, though *Jensen et al.* [1999] deduce such information by use of MLS and CLAES data together.

The most recent MLS data version (V490) has been used to analyze zonal mean behavior of water vapor [*Sandor et al.,* 1998], longitudinally resolved spatial distributions [*Stone et al.,* 2000], and are used in this paper. CLAES cirrus measurements, derived from version 8 (V8) aerosol extinctions, are described by *Mergenthaler et al.* [1999]. They find good agreement between the CLAES data and the 1985-1990 SAGE II tropical subvisible cirrus climatologies [*Wang et al.*, 1995]. The CLAES cirrus cloud and MLS upper tropospheric humidity data sets contain 431 days of coincident measurements during UARS days 40-602 (Nov91-May93).

3. Data Analysis

147 hPa data were placed in bins of 5° latitude, 10° longitude, and by season. Within each bin, the MLS RHI values for which there were coincident CLAES aerosol extinction measurements were averaged. Cirrus clouds were considered to be present for CLAES 780 nm spectrometer aerosol extinction values greater than 0.9×10^{-3} km^{-1}, and absent otherwise, the same criterion used by *Mergenthaler et al.* [1999]. CLAES is sensitive to visible as well as subvisible clouds. However, we interpret the CLAES detected clouds to be primarily subvisible clouds (see section 2). Percent cloudiness within each geographic/seasonal bin was calculated as the fraction of CLAES extinction measurements greater than 0.9×10^{-3} km^{-1}. Figure 1 is a scatterplot of the fractional cloudiness vs. MLS RHI values for latitudes 20°S-20°N. This includes 8 latitude × 36 longitude × 4 seasonal bins, for a total of 1152 data points. A cubic fit to the data is plotted as a solid line, and the dashed lines indicate $\pm1\ \sigma$ from the best fit.

The offset between CLAES and MLS measurements (<30 seconds, <200 km) is small relative to our geographic bins, but can be large compared with the spatial scale of cirrus and RHI variability. A profile by profile scatter plot of CLAES extinction vs. MLS RHI [*W.G. Read et al., manuscript in preparation,* 2000] shows a wider spread than that shown in fig. 1. This difference in scatter is associated with the different spatial scales, and with reduced random error due to averaging over multiple measurements. Fractional cloudiness (fraction of CLAES observations in which clouds are detected) drops to zero as mean RHI values decrease to 35%. Low RHI measurements at 147 hPa are unusual for 20°S-20°N, in agreement with the 10°S-10°N *Jensen et al.* [1999], and 30°S-30°N *Sandor et al.* [1998] analyses. Inclusion of drier measurements by extending the latitude range to 40°S-40°N (not shown) gives a functional dependence indistinguishable as that of fig. 1, except for a dry tail, deviating significantly to the left of the 20°S-20°N behavior only for less than 10% cloud occurrence, and crossing the x-axis at 10% RHI.

Figure 1a shows there is negligible seasonal variation of the cloudiness vs RHI relationship. Best fits of each season's data fall well within the 1-σ scatter of the 12-month data. Figure 1b similarly shows there is little longitudinal variation of the cloudiness vs RHI relationship. Longitude bins depicted in fig. 1b are 0°-45° (Africa), 90°-180° (wet western Pacific), 210°-270° (dry eastern Pacific) and 285°-300° (South America). These were chosen to contrast wet with dry regions of the Walker circulation, as well as continental with oceanic areas. Best fits to each longitude bin's data are within the 1-σ scatter of the 360° data. The only exception is the small domain drier than RHI=30%, cloudiness=10% for 285°-300° (South America).

CLAES data have been filtered by the *Mergenthaler et al.* [1999] overhead cloud clearance criteria: In altitude profiles where a cloud is detected at 100 or 68 hPa, with extinction uncertainty >30%, the 147 hPa measurement is discarded. The effect of this CLAES data

filter on the cloudiness vs RHI relationship is small, but is included in our analysis.

4. Interannual Variability

One value of establishing an RHI-cloudiness relationship is that cloudiness may be inferred for the period of MLS operation following the end of CLAES measurements. Interannual changes in tropical Pacific upper tropospheric humidity associated with El Nino are seen in the MLS data [*Waters et al.*, 1999, their Fig. 14]. Here we discuss differences in geographic distribution of cloudiness between years of strong and weak El Nino.

Figure 2 shows the mean regional distribution of thin cirrus for each of the years 1992 to 1996. Annual means are over the period Dec. 1 - Nov. 30. The monotonic increase in cirrus frequency with increase of average RHI (fig. 1) means the cirrus occurrence patterns (fig. 2) are similar to RHI geographic distributions on this surface. The small scatter in fig. 1 (1σ =10%) means the cirrus frequency values in fig. 2 are quantitatively reliable, with uncertainty of the rms sum of 10% (due to fig. 1 scatter) and uncertainty inherent in the CLAES observations themselves. CLAES regional seasonal cloud occurrence at 147 hPa agrees with SAGE II climatology within 16% [*Mergenthaler et al.*, 1999].

Changes in thin cirrus distribution associated with El Nino are apparent (fig. 2) in comparison of years 1992-93 (moderately strong warm phase) with years 1995-96 (neutral to weakly cold phase). During warm phase years there is increased cloudiness throughout the Pacific (except at a localized minimum near 130°E), with an eastward shift of maximum tropical cloudiness in the western Pacific, and near-zero area of minimum ($\leq$8%) cloud occurrence in the eastern Pacific. This is consistent with eastward shifting of convective cloud cover [*Chen and Houze*, 1997], and of upper tropospheric water vapor [*Waters et al.*, 1999] during El Nino. Our annual-mean analysis (fig. 2) is similar to the *Mergenthaler et al.* [1999] seasonal comparisons of Dec-Feb 1991-92 (peak of the 1991-93 El Nino) CLAES data, Dec-Feb 1992-93 (moderate strength El Nino) CLAES data, and the 1985-90 SAGE II seasonal climatology: CLAES data during the strong El Nino show more cirrus in the Pacific than during moderate conditions. Additionally, *Mergenthaler et al.* [1999] show strong El Nino CLAES cirrus is shifted eastward in the western Pacific and has a diminished area of minimum prevalence in the eastern Pacific, relative to both moderate El Nino CLAES cirrus and to 1985-90 SAGE II climatology. The MLS El Nino local minimum near 130°E (fig. 2) is also seen in convective clouds [*Chen and Houze*, 1997, their plate 1] during El Nino Nov-Feb 1986-87, and in CLAES cirrus [*Mergenthaler et al.*, 1999] near 160°E during El Nino Dec-Feb 1991-92.

In the western Pacific, 1994 shows a transition from the 1993 El Nino to more neutral conditions in 1995. 1994 also has less tropical cirrus than in any other year; this will be a subject of future investigations.

5. Summary

We use coincident measurements of upper tropospheric RHI (with MLS) and of cirrus ice (with CLAES) to demonstrate and quantify a strong correlation between the seasonal geographic means of tropical water vapor and occurrence frequency of thin (often subvisible) cirrus at 147 hPa (fig. 1). We emphasize that this correlation is quantitatively useful only for averages over many measurements. Use of a single MLS measurement of RHI (to infer presence or absence of cirrus at a specific time and place) is not addressed in this study. Monotonic increase of cirrus occurrence frequency with increasing RHI implies that changes in mean RHI are mirrored by changes in cirrus frequency. With the (fig. 1) cirrus vs RHI relationship, we use MLS RHI as a proxy measure of cloud occurrence for Sept 1991 - June 1997, extending well beyond the 19 month CLAES lifetime. Interannual changes in the geographic distribution of cirrus occurrence (fig. 2) are evident in the tropics. Much of this variation is associated with El Nino: High frequencies of cirrus occurrence are shifted eastward during El Nino's warm phase, similar to eastward displacements of water vapor and lower altitude clouds.

The importance of thin cirrus in the tropical radiation budget, and hence in climate modeling, was demonstrated in detail by *Jensen et al.* [1999]. Proxy measures of cirrus behavior (e.g. fig. 2), as well the empirical relationship between cirrus and RHI (fig. 1) may be compared with climate model calculations, potentially serving as diagnostics of those models.

Our 147 hPa 20°S-20°N analysis can be extended to 40°S-40°N. The 40°S-40°N cirrus occurrence vs mean RHI relationship (not shown) differs significantly from that for 20°S-20°N (fig. 1) only for cloud occurrence <10% - a domain poorly represented equatorward of 20°. Simultaneous CLAES cloud and MLS water vapor data are available at 215 hPa, and it is likely a similar

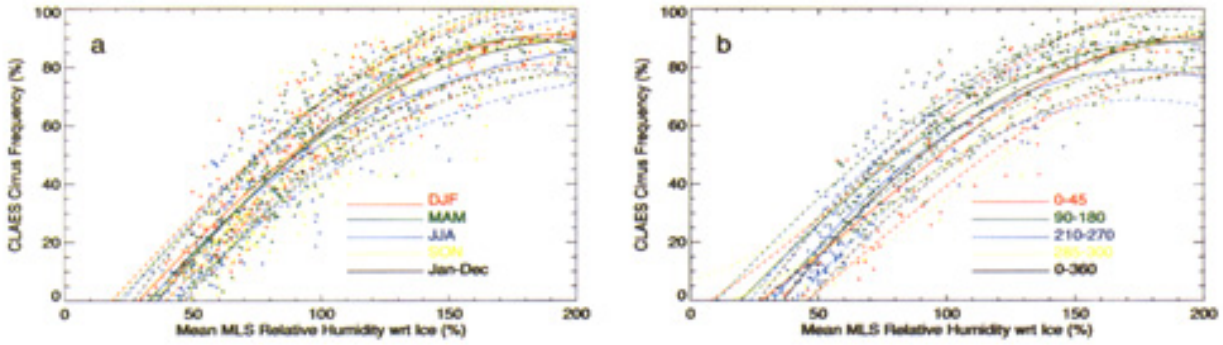

Figure 1. Percent of CLAES observations that detect cirrus as a function of mean MLS-measured RHI. (MLS RHI>100% should not be interpreted in terms of supersaturation. See text section 2.) Each data point represents a seasonal (3 month) mean value for an area 10° longitude x 5° latitude, and equatorward of 20°. The black solid line is a polynomial fit to all these data. Colors in (a) show data according to season. Red: Dec.-Feb. (DJF); Green: Mar.-May (MAM); Blue: June-Aug. (JJA); and Yellow: Sept.-Nov. (SON). Colors in (b) show data binned by longitude. Red: 0°-45° (Africa); Green: 90°-180° (wet western Pacific); Blue: 210°-270° (dry eastern Pacific); and Yellow: 285°-300° (South America). Fig. 1 demonstrates that the tropical subvisible cirrus vs RHI relationship is independent of season and of longitude. Dashed lines indicate ± 1-σ deviation from the best fit.

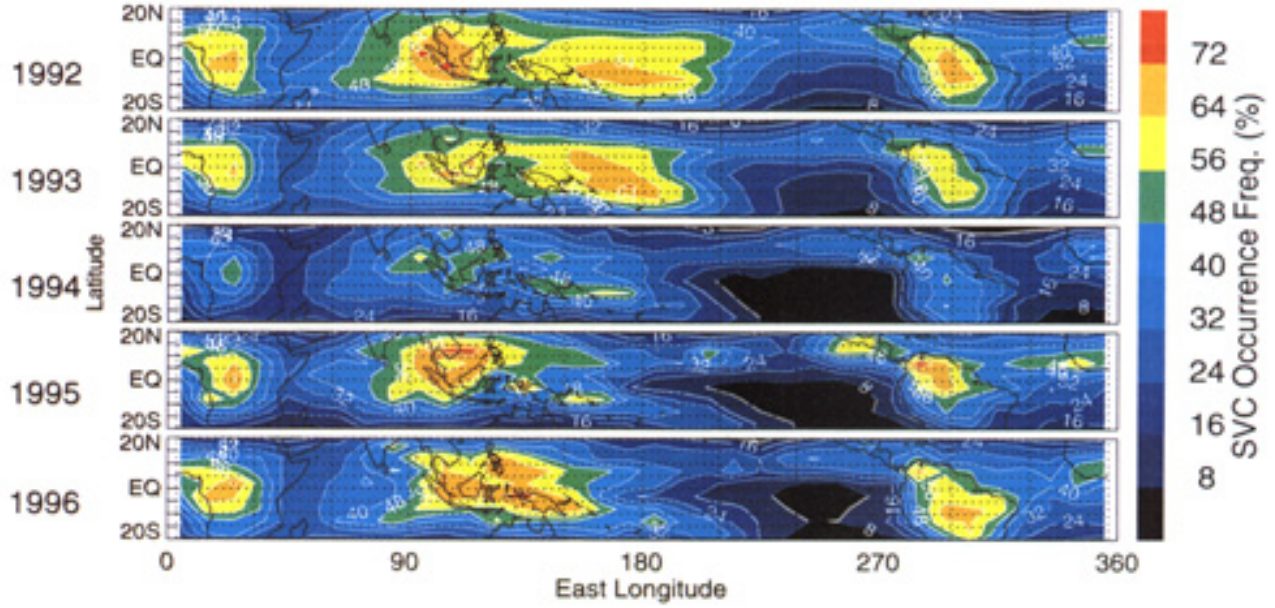

Figure 2. Frequency of subvisible cirrus for years 1992-96. Cloud frequency is calculated from MLS RHI observations and the cloud occurrence vs RHI relationship shown in fig. 1. El Nino effects are seen most strongly in the Pacific, which has more cirrus during warm phase years 1992-93 than in neutral years 1995-96.

relationship exists there for some latitude range. We are currently investigating this possibility. The (fig. 1) CLAES vs MLS relationship should hold qualitatively for other instrument pairings, but new quantitative comparisons need to be made for other instruments. As an example, EOS MLS [*Waters et al.*, 1999] and EOS HIRDLS [*Edwards et al.*, 1995] will each measure water vapor and cirrus, though in different altitude and abundance regimes, from a single spacecraft. Measurement intercomparison will give functional dependencies similar to fig. 1 for various data product pairings, enabling a better understanding of cirrus over a wide range of conditions. If one of the instruments outlives the other, proxy extension of the short-lived with the long-lived instrument should be possible, as we have proxy-extended the CLAES measurements with UARS MLS.

Acknowledgments. We thank Steve Massie, Bill Randel and Anne Smith for scientific discussions. The National Center for Atmospheric Research is supported by the National Science Foundation.

References

Barath, F.T., et al., The Upper Atmospheric Research Satellite Microwave Limb Sounder instrument, *J. Geophys. Res., 98,* 10,751-10,762, 1993.

Chen, S.S., and R.A. Houze, Jr., Interannual variability of deep convection over the tropical warm pool, *J. Geophys. Res., 102* 25,783-25,795, 1997.

Edwards, D., et al., Selection of the sounding channels for HIRDLS, *Appl. Opt., 34* 7006-7017, 1995.

Jensen, E.J., et al., High humidities and subvisible cirrus near the tropical tropopause, *Geophys. Res. Lett., 26,* 2347-2350, 1999.

Jones, R.L., and J.F.B. Mitchell, Is water vapour understood?, *Nature, 353,* 210, 1991.

Massie, S.T., et al., The effect of El Nino on the distribution of tropical cirrus, *J. Geophys. Res., submitted,* 2000.

Mergenthaler, J.L., et al., CLAES observations of tropical cirrus, *J. Geophys. Res., 104,* 22,183, 1999.

Read, W.G., et al., Upper tropospheric water vapor from UARS MLS, *Bull. Am. Meteorol. Soc., 76,* 2381, 1995.

Roche, A.E., et al., The Cryogenic Limb Array Etalon Spectrometer (CLAES) on UARS: Experiment description and performance *J. Geophys. Res., 98,* 10,763-10,776, 1993.

Sandor, B.J., et al., Seasonal behavior of tropical to mid-latitude upper tropospheric water vapor from UARS MLS, *J. Geophys. Res., 103,* 25935-25947, 1998.

Sassen, K., and B.S. Cho, Subvisual-thin cirrus lidar dataset for satellite verification and climatological research, *J. Appl. Meteor., 31,* 1275-1285, 1992.

Stone, E.M., et al., Spatial distributions of upper tropospheric water vapor measurements from the Microwave Limb Sounder, *J. Geophys. Res., 105,* 12149, 2000.

Udelhofen, P.M., and D.L. Hartmann, Influence of tropical cloud systems on the relative humidity in the upper troposphere, *J. Geophys. Res., 100,* 7423-7440, 1995.

Wang, P.-H., et al., A 6-year climatology of cloud occurrence frequency from SAGE II observations (1985-1990), *J. Geophys. Res., 101,* 29407-29429, 1996.

Warren, S.G., et al., Global distribution of total cloud cover and cloud type amounts over land, *NCAR TN-273+STR,* Natl. Cent. for Atmos. Res., Boulder, CO, 1986.

Warren, S.G., et al., Global distribution of total cloud cover and type amounts over ocean, *NCAR TN-317+STR,* Natl. Cent. for Atmos. Res., Boulder, CO, 1988.

Waters, J.W. et al., UARS and EOS microwave limb sounder (MLS) experiments, *J. Atmos. Sci., 56,* 194, 1999.

E.J. Jensen, E.M. Stone, NASA Ames Research Center, MS 245-4, Moffett Field, CA 94035.

J.L. Mergenthaler, Lockheed Palo Alto Research Laboratory, 3251 Hanover Street, Org. 91 20, Bldg. 252, Palo Alto, CA 94304.

W.G. Read, J.W. Waters, JPL, MS 183-701, 4800 Oak Grove Drive, Pasadena, CA 91109.

B.J. Sandor (corresponding author), Space Science Institute, 3100 Marine Street, Suite A353, Boulder, CO 80303-1058. (email: sandor@gemelli.colorado.edu)

(Received October 20, 1999; revised March 9, 2000; accepted May 16, 2000.)